https://doi.org/10.26552/aer.C.2020.2.2

STUDY OF REINFORCEMENT DESIGN H-PROFILE OF AIRCRAFT WING SPAR

Pavol Pecho
Air Transport Department
University of Zilina
Univerzitná 8215/1
010 26, Žilina
Pavol.pecho@fpedas.uniza.sl

Paulína Magdolenová
Department of Fire Engineering
University of Zilina
Univerzitná 8215/1
010 26, Žilina
Paulina.magdolenova@kpi.fbi.sk

Michal Hrúz
Air Transport Department
University of Zilina
Univerzitná 8215/1
010 26, Žilina
michal.hruz@stud.uniza.sk

Pavel Kováčik
Kobaltsky Welding
Jerichov 26
957 01, Brezolupy
Kobaltsky1@gmail.com

Iveta Škvareková
Air Transport Department
University of Zilina
Univerzitná 8215/1
010 26, Žilina
Iveta.skvarekova@fpedas.uniza.sk

Abstract

In today's world, with ever-increasing safety requirements, there is a growing demand to maintain or reduce production costs. In aviation, in addition to factors like weight and related variables such as resistance to vibration, corrosion, temperature and other are also considered. The task of this paper is to analyse unconventional designs of wing beams with respect to the current requirements of the aviation industry. In the article, the authors analyse the possibilities of design modification either by adding ribs to the profile, or by changing the cross-section of the profile itself. In practice, such design changes would increase weight, production time and finances, but also increase strength and thus safety. All proposed changes were subjected to strength analyses by FEM (Finite element method) computer simulations. The article output is the selection of suitable designs for further observation and experimental verification to ensure comprehensive results for the possibility of implementation in practice. Despite the non-traditional shapes of the proposed wing beam cross-sections, the authors assume that traditional beam shapes will be gradually modified more efficiently.

Keywords

wing spar, wing beam, H-profile, wing design

1. Introduction

Historically, the first flight dates back more than 100 years. Even then, aircraft designers were looking for ways to build solid wings. However, in terms of beam strength, the problem is much older. Beams are the basic element of the longitudinal system of the wing. In the case of purely girder wings, they ensure the full extent of the transmission of bending loads; in the case of girder half-shells, they play a significant role in the bending transmission (Kindmann, 1993). Their weight is in the range of 25 - 50% of the whole wing weight, while higher values relate to beam wings, lower values to half-shells wings (Chen, C.-C, 2019). According to the structural arrangement, we divide the beams into full-walled and, rarely occurring, lattice beams. Like in aviation, as well as in the civil engineering industry beam with I- or H-profile occur. The area of building constructions inspired authors with the ability to drop the collapse risk by adding supporting elements to the beams, for example in the form of ribbing (Figure 1-right) (Abdel-Ghaffar, 2003). The ribbing allows a more efficient distribution of internal material stresses and prevents the beam from collapsing (Figure 1-left).

Figure 10: Detail of the numerical simulation of the steel column collapse with additional ribbing (left) and additional ribs on steel H-profile building structure beam (right). Source: Authors.

In both fields, civil and aerospace engineering, the main effort is focused on prevention of bursts, collapse, or any other damage. To ensure the best mechanical properties, it is necessary to know the position of a beam neutral axis. The neutral axis is a line (more precisely in the spatial concept of the area), which changes the sense of its internal axial effective countervailing forces under bending stress (Figure 3). That means that the best use of the mechanical properties of the beam flange material is in the places furthest from its neutral axis (Nardin, 2009).

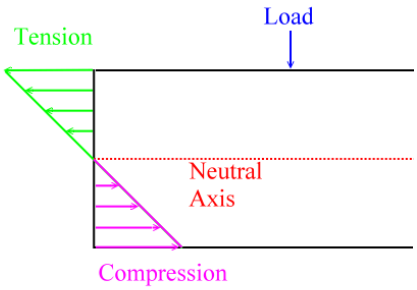

Figure 11: Visualization of the neutral axis at the side looking at the H-profile beam source: Authors.

Assuming the use of the same material and of the same cross-section for both the upper and the lower flange, the neutral axis will lie in the middle of the beam height. For most of the wing beams is, indeed, the material of the two flanges is the same, but usually with different cross-sections. The neutral axis then passes through the common gravity centre of these two flanges and it tends to be closer to the thicker, predominantly of the upper flange (Starší, 2020).

The figure 3 shows a metal embedded beam of a Bf-109 fighter aircraft. The beam has, for the most part of the span, a profile I, near the end of the wing it passes into a profile C. The flanges (1) are made of duralumin L-profiles (3), the cross-section of which decreases towards the wing end. The web (2) is made of duralumin sheet, in the root part thicker, at the end of the wing the sheet is thinner. The rear flange (pictured from the visible side of the beam) degrades from its L-profile to its end in the area between sections A and C only into a vertical shear plate riveted to the web. The front L-profile is terminated even earlier than the rear and passes into the sheet metal flange of the wing end, which is formed by bending the end part of the web into a C-shape. The hinge fittings (5) are made of high-strength steel. The lower hinge is equipped with a ball joint both to reduce the parasitic load on the hinges by operational deformations of the spar, and to facilitate its assembly and disassembly. A number of spacers (6) are arranged along the length of the beam to reinforce the web. These are also used to connect the ribs to the beam. It is worth mentioning the reinforcement (9) of the web in the place of the large hole, which was forced by the cannon installation in the wing. The view of the entire skeleton of the wing is also shown in the Figure 3. The front L-profile is terminated even earlier than the rear and passes into the sheet metal flange at the wing end, which is formed by bending the end portion of the web into the C-shape (Starší, 2020).

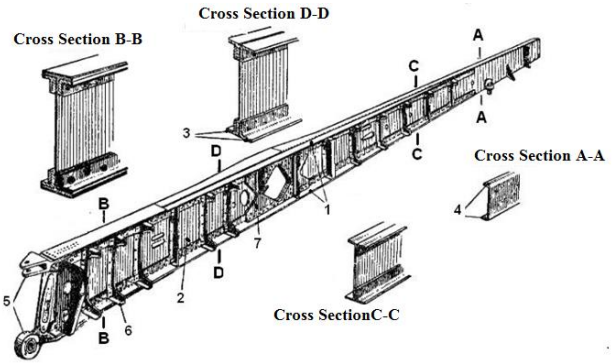

Figure 12: Wing spar of BF-109 airplane. Source: Starší (2020).

Along with the size and shape of the flange cross-section, the mechanical properties of the used material, namely its tensile modulus E, contribute to the final beam stiffness (Chu AYT, 2002). In the following chapters we will go through an analysis of proposed new beam types and their properties with respect to the requirements of the smallest possible stress under load and the smallest possible weight.

2. Materials & Methods

The study focused on the strength analysis of different wing beam is divided into two basic groups. In both cases the beams are the H-profile, but the changes are in additional elements, ribs or in the cross-section shape of the beams. All designs are based on the basic proposal, which shape and dimensions in millimetres are below in the figure 4. Total length of beams is 1500 mm.

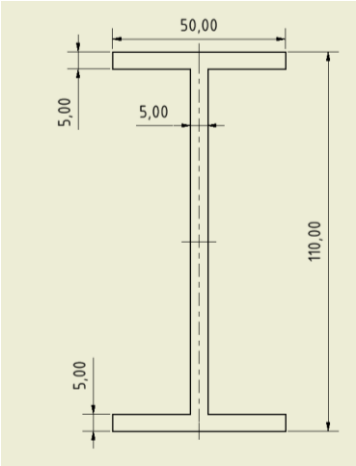

Figure 13: Cross-section dimensions of basic beam for numerical simulations. Source: Authors.

The material of the simulated beams is the Aluminium 6061 „Dural“ with common use in the aviation industry. During the simulations the beams were fixed at one of the ends and loaded with a steady force with different values on the upper beam flange. In the first group of beams were those that were supplemented by ribbing. The following figure 5 shows the first group. From top to bottom goes first the ordinary beam with the dimensions according to the figure 4, followed by the beam with transverse ribbing, the beam with ribs at an angle of 45 ° to each other and the last beam with parallel ribbing at an angle of 45 °.

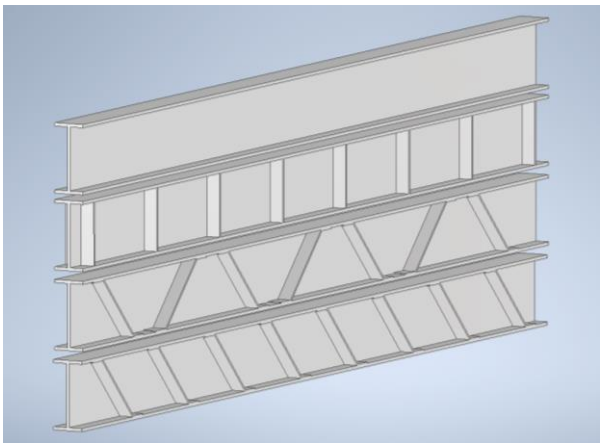

Figure 14: Group of tested beams with additional ribbing. Source: Authors.

Taking into account, the properties of the neutral axis and the danger of deformation of the beam wall, the authors investigated the modifications by additional elements with creating different cross-sections. The following Figure 6 shows the types of the beams that were examined.

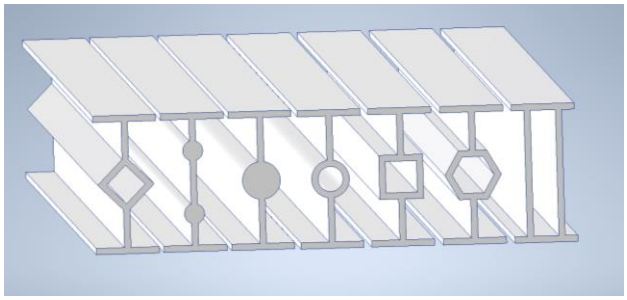

Figure 15: Cross-section patterns used for numerical simulations (from left to right – diamond, full dual „o“, full „o“, hollow „o“, rectangular, hexagonal, dual beam. Source: Authors.

The figure 6 Cross-section patterns used for numerical simulations (from left to right – diamond, full dual „o“, full „o“, hollow „o“, rectangular, hexagonal, dual beam

The numerical analysis was divided into a total of 16 parts and 4 different loads were applied for each beam type, which were graduated from 200 N, 400 N, 600 N to 800 N. The load was applied perpendicular to the top of the beam as shown in the figure 7.

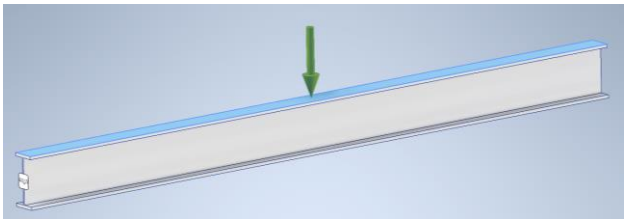

Figure 16: Beam attachment and direction and distribution of the applied force. Source: Authors.

The figure 7 Beam attachment and direction and distribution of the applied force

The results of numerical simulations were evaluated from three different points of view. These were the Von Mises Stresses (MPa), displacements (mm) and the weight (kg) of the currently simulated beam. The simulations were performed with Autodesk Inventor 2020 software using the strength analysis function. The average size of the element (as a length fraction of the bounding polygon) at network formation was 0.5. As already mentioned, the material in the simulations was chosen aluminium with the designation 6061, also known as “Dural”. An overall view of the basic beam simulation is shown in the figure 8.

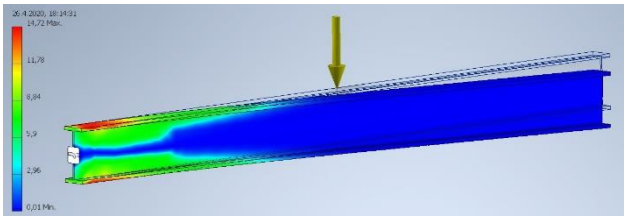

Figure 17: A view of the basic beam bending simulation with the course of Von Mises Stress (MPa). Source: Authors.

3. Results

The results of the simulations are shown in Table 1. From this table it is clear that when comparing the weight, the first group of beams was lighter than the second group. From the point of view of displacement evaluation and internal stresses, however, the results were opposite. The computational simulations show (Table 1) that the best rated beams include “dual beam” and “full dual “o””. For this reason, the team of authors focused on further monitoring the properties of these beams by their combination or dimensional modification, while maintaining a weight of approximately 5 kilograms.

Table 2: Numerical simulation results of beam designs. Source: Authors.

Beam	Max. Displacement 200N (mm)	Max. Tension 200N (Mpa)	Max. Displacement 400N (mm)	Max. Tension 400N (Mpa)	Max. Displacement 600N (mm)	Max. Tension 600N (Mpa)	Max. Displacement 800N (mm)	Max. Tension 800N (Mpa)	Weight (kg)
Additional Ribs									
No Ribs	0,691	4,986	1,384	9,972	2,076	14,96	2,767	19,94	4,05
Cross Ribs	0,685	4,715	1,37	9,43	2,055	14,15	2,74	18,86	4,342
Inclined opposite Ribs 45°	0,617	5,185	1,342	10,37	2,013	15,56	2,684	20,74	4,485
Inclined Parallel Ribs 45°	0,67	6,028	1,34	12,05	2,01	18,08	2,68	24,11	4,548
Profile Change									
Dual Beam	0,557	3,898	1,115	7,796	1,672	11,69	2,229	15,59	6,075
Hollow "O"	0,6863	5,094	1,373	10,19	2,059	15,28	2,745	20,38	5,036
Full "O"	0,678	4,847	1,356	9,692	2,035	14,54	2,713	19,39	6,308
Full dual "O"	0,636	4,72	1,272	9,439	1,908	14,16	2,544	18,88	5,041
Rectangular	0,663	4,755	1,326	9,509	1,989	14,26	2,652	19,02	5,771
Diamond	0,671	4,842	1,354	9,683	2,031	14,52	2,709	19,37	5,362
Hexagonal	0,664	4,78	1,328	9,559	1,992	14,34	2,656	19,12	5,644

Through gradual analysis, we came to the fact that the direct displacement of the elements closer to the flanges affects the overall rate of stresses and displacements under load. The final proposal (Figure 9(b)) is designed so that the “o” elements are shifted to the closest possible distance to the flanges, therefore 43 mm from the centre of the beam. This distance was chosen because of the space for the placement of the structure welds. In addition to this design, another model was investigated with the ribs addition perpendicular to the beam wall (Figure 9(a)).

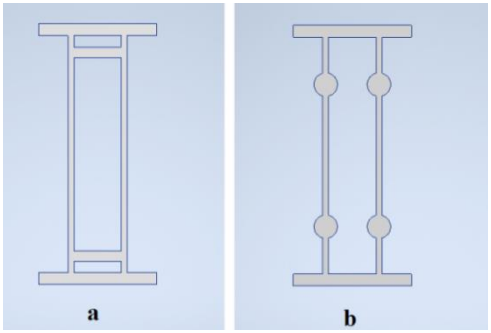

Figure 18: Visualization of improved and final beam designs - Dual Beam (half thickness) + middle ribs 43mm from center (a), Dual Beam (half thickness) + dual full "O" 43mm from center (b). Source: Authros.

The following Table 2 evaluates the numerical simulations of the additional designs. The final designs from the figure 9 are in the penultimate and last place in Table 2.

Table 3. Numerical simulation results of additional beam designs. Source: Authors.

Beam	Max. Displacement 200N (mm)	Max. Tension 200N (Mpa)	Max. Displacement 400N (mm)	Max. Tension 400N (Mpa)	Max. Displacement 600N (mm)	Max. Tension 600N (Mpa)	Max. Displacement 800N (mm)	Max. Tension 800N (Mpa)	Weigh t (kg)
Dual Beam (half thickness)	0,69	4,634	1,381	9,268	2,072	13,09	2,763	18,54	4,05
Dual Beam (half thickness) + dual full "O"	0,643	4,747	1,326	10,05	1,93	14,26	2,574	18,99	4,922
Dual Beam (half thickness) + dual full "O" 30mm from center	0,624	4,652	1,25	9,302	1,875	13,96	2,499	18,69	4,922
Dual Beam (half thickness) + dual full "O" 43mm from center	0,576	4,276	1,135	8,553	1,703	12,83	2,27	17,11	4,922
Dual Beam (half thickness) + middle ribs 43mm from center	0,583	4,035	1,168	8,071	1,752	12,11	2,336	16,14	4,779

It is obvious from the design that the additional ribbing and elements influenced the stress distribution in the materials. From the figure 10 (top) it can be determined that the design "Dual Beam (half thickness) + middle ribs 43 mm from centre" has a more even distribution of the stresses across the cross-section. In the proposal "Dual Beam (half thickness) + dual full" O "43 mm from centre" are the stress and forces carried by extra "O" elements in the cross-section. Authors also created combinations of the designs, but numerical simulations did not show significant improvements over the original designs

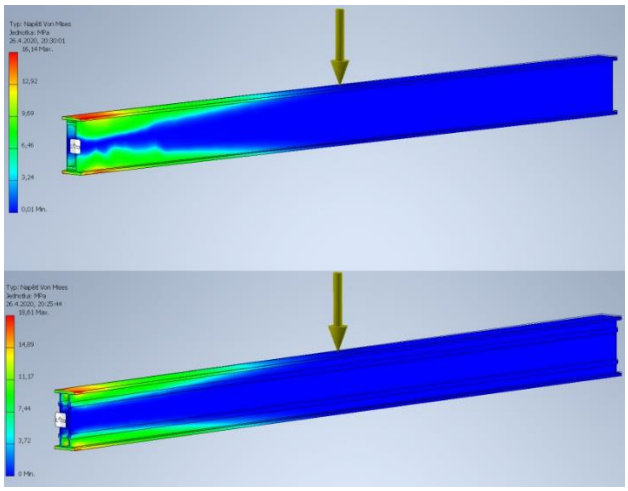

Figure 19: Visualization of the final beam designs with a distributed 800 N load. Dual Beam (half thickness) + middle ribs 43 mm from centre (upper part), Dual Beam (half thickness) + dual full "O" 43 mm from centre (lower part). Source: Authors.

The overview of selected design results is shown in the Graph 1, which contains proposals from Tables 1 and 2. The designs in the Graph 1 are numbered in ascending order from Table 1 (1-11) and Table 2 (12-16). From Graph 1 it is clear that the best strength characteristics has the design no. 5, i.e. "Dual Beam". Nevertheless, this beam has 16% more weight than the rest. For this reason, this design is inappropriate. From this point of view, however, it is necessary to consider the overall behaviour and susceptibility to fatigue and cracks (Čerňan, 2019).

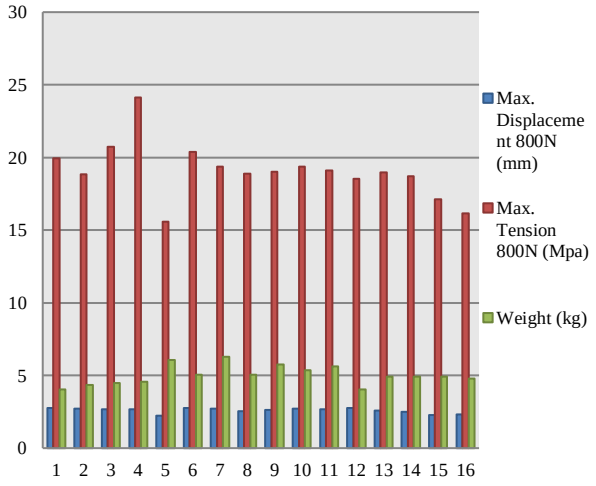

Graph 1: Comparison of Max. Displacement (mm) and Max. Tension (MPa) under 800 N load beside of total weight of beams. Source: Authors.

From the comparison of the other beams, the final properties from the figure 9 had the best properties. Therefore, these proposals were evaluated for further research and experimental validation. In addition to the designs, it is necessary to take into account the possibility of corrosion (Janovec, 2020) and fatigue wear. (Čerňan, 2018) In particular, wall thickness is prone to dimensional changes due to corrosion and cracks. However, the use of modern NDT diagnostic methods solves this problem (Janovec, 2019).

4. Conclusion

The study of the beam numerical simulations was focused on the design possibilities of increasing the wing structure strength. By performed simulations, it was possible to determine the beams with the best results, and subsequently to modify and optimize these designs. The study result are two designs of the H-profile with the double wall and additional elements as shown in the Table 2 and the Graph 1. Current designs are still the subject of research and appropriate optimization for further research. The given results can be experimentally verified and thus prove the correctness of numerical simulations. During the design process, the authors also tried to take into account the production technology of the given beams and the proposed designs to meet sufficient criteria for fast and efficient construction. In the case of the successful experimental verification, these optimized beams would be suitable in the wing construction use and could be considered to be used also in civil engineering, where the inspiration came from.

Acknowledgment

This work was supported under the project of Operational Programme Integrated Infrastructure: *Research and development of contactless methods for obtaining geospatial data for forest monitoring to improve forest management and enhance forest protection*, **ITMS code 313011V465**. The project is co-funding by European Regional Development Fund.

References

Abdel-Ghaffar, M.M.E., April 2003, "Limit-Load Analysis vs. Destruction Testing of Perforated Cold Formed Steel Cable Trays", 10th International Colloquium on Structural and Geotechnical Eng., Ain-Shams Univ., Egypt, ST02, pp.1-12.

Beňo, L., Bugaj, M., & Novák, A. 2005. Application of RCM principles in the air operations. Komunikacie, 7(2), 20-24.

Čerňan, J., Janovec, M., Hocko, M., Cúttová, M., 2018. Damages of RD-33 Engine Gas Turbine and their Causes. Transportation Research Procedia 35, 200–208. https://doi.org/10.1016/j.trpro.2018.12.028

Čerňan, J., Semrád, K., Draganová, K., Cúttová, M., 2019. Fatigue stress analysis of the DV-2 engine turbine disk. Aircraft Engineering and Aerospace Technology 91, 708–716. https://doi.org/10.1108/aeat-03-2018-0096

Chen, C.-C., Sudibyo, T., 2018. Effect of Intermediate Stiffeners on the Behaviors of Partially Concrete Encased Steel

Beams. Advances in Civil Engineering 2018, 1–15. https://doi.org/10.1155/2018/8672357

Chu AYT, Chan SL, Chung KF., 2002, “Stability of modular steel scaffolding systems - theory and verification. Proceedings of International Conference Advances in Building Technology Hong Kong”.

Janovec, M., Čerňan, J., & Škultéty, F. (2020). Use of non-destructive eddy current technique to detect simulated corrosion of aircraft structures. Koroze a Ochrana Materialu, 64(2), 52–58. https://doi.org/10.2478/kom-2020-0008

Janovec, M., Smetana, M., Bugaj, M., 2019. Eddy Current Array Inspection of Zlin 142 Fuselage Riveted Joints. Transportation Research Procedia 40, 279–286. https://doi.org/10.1016/j.trpro.2019.07.042

R. Kindmann, R. Bergmann, L. G. Cajot, and J. B. Schleich, “Effect of reinforced concrete between the flanges of the steel profile of partially encased composite beams,” *Journal of Constructional Steel Research*, vol. 27, no. 1–3, pp. 107–122, 1993.

S. D. Nardin and A. L. H. C. Debs, “Study of partially encased steel composite beams with innovative position of stud bolts,” *Journal of Constructional Steel Research*, vol. 65, no. 2, pp. 342–350, 2009.

Starší, D., 2020. O Letadlech - Dušan Slavětínský Starší - Konstrukce Nosníku. [online] Slavetind.cz. Available at: <http://www.slavetind.cz/stavba/konstrukce/kridlo/Konstr_nosniku.aspx> [Accessed 2 May 2020]